Lyle, M., Wilson, P.A., Janecek, T.R., et al., 2002
Proceedings of the Ocean Drilling Program, Initial Reports Volume 199

3. Straw Man 1: A Preliminary View of the Tropical Pacific from a Global Coupled Climate Model Simulation of the Early Paleogene[1]

Matthew Huber[2]

ABSTRACT

A coupled ocean-atmosphere climate model is used to provide concrete predictions of climate properties and processes in the eastern tropical Pacific during the early Paleogene in equilibrium with 560 ppm pCO_2. This climate model simulation provides estimates of upwelling, temperature, current velocities, thermocline tilt, and salinity (independent of climate proxy interpretations) to provide a framework for comparison with Leg 199 data. The simulated east-west temperature gradients are comparable, although somewhat (~2°C) stronger, to modern temperature gradients, with vigorous upwelling in the eastern equatorial Pacific. Near-surface and intermediate-depth current structures are extremely variable, both spatially and temporally, making generalizations about current directions and strengths difficult. A North Atlantic water mass traveling through the open Panamanian Isthmus at intermediate to deep levels in the equatorial Pacific provides a signal of "young" water at depth at the location of Leg 199 sites. Estimates of seawater and calcium carbonate oxygen isotopic compositions are also made. Some implications of possible differences between findings based on data from Leg 199 and this modeling study are briefly discussed.

[1]**Examples of how to reference the whole or part of this volume.**
[2]Danish Center for Earth System Science, Niels Böhr Institute, Denmark. **rop@dcess.ku.dk**

Ms 199IR-103

INTRODUCTION

It is not customary to perform paleoclimate modeling hand in hand with data collection. The separation of data collection and modeling is generally beneficial, but for this particular problem—characterizing the tropics in a poorly understood time interval and clarifying the relationship between the tropics and global climate—it is appropriate to make an exception. This cruise and its companion (Ocean Drilling Program [ODP] Leg 198 to Shatsky Rise) are not the first to collect data on the early Paleogene tropical climate. Rather, these cruises returned to answer questions that have plagued the early Paleogene community for almost two decades. It is important to note that climate models themselves have evolved recently. We can now make predictions that are entirely independent of climate proxies because stable, fully coupled, comprehensive (atmosphere-ocean-land surface-sea ice), and well-validated climate models are now available. Results from these paleoclimate modeling studies allow us to construct a "straw man" for the sake of clarifying the differences between what climate proxies tell us and what, based on well-understood physical processes, we expect.

The early Paleogene is usually characterized as having near-modern (~25°C) tropical sea-surface temperatures (SSTs) and warm winters in extratropical continental interiors. Together, these features have proven difficult to reconcile with our current understanding of climate (Barron, 1987; Sloan and Barron, 1990; Wolfe, 1994; Zachos et al., 1994; Bralower et al., 1995; Greenwood and Wing, 1995). Existing tropical SST reconstructions may not, however, necessitate a fundamental rethinking of climate dynamics because

1. The spatial distribution and temporal evolution of early Paleogene tropical SSTs have not been clearly established (e.g., Crowley and Zachos, 2000);
2. The little high-resolution proxy data collected suggest substantial variability in early Paleogene tropical SSTs (Bralower et al., 1995); and
3. The uncertainties in early Paleogene tropical SST proxy interpretation are large (~2°–7°C) and potentially systematically biased to cool values (Schrag, 1999; Huber and Sloan, 2000; Pearson et al., 2001, and references therein).

WHY USE A STRAW MAN MODEL?

The most robust characterizations of paleoclimates are established when multiple proxies are present for the same climate characteristic. Where proxies disagree or multiple proxies are unavailable, as has been the case for Paleogene tropical SSTs, the climatic interpretation becomes muddied. As exemplified by the debate over tropical SSTs at the last glacial maximum, models or theory might shed some light, but only the collection of more proxy records is likely to resolve the issue. Nevertheless, great leaps in understanding occur only in situations in which theories and models fail to match key data. This requires theories and models that are independent of the data, to avoid circularity. This is the special purpose of having a null hypothesis and a straw man model.

In the past, it has been difficult to provide such a straw man because climate models have required either a specified SST or heat flux distri-

bution as input. Thus, attempts to answer the question of what maintains the temperature and heat flux distributions become entangled in circular reasoning. In these models (summarized in DeConto et al., 2000), the surface freshwater balance is also not given a self-consistent treatment because realistic ocean-atmosphere interactions are not included. Uncoupled modeling efforts have been hampered by the fact that they must explicitly incorporate either assumptions based on modern-day relationships (e.g., modern ocean heat flux) or existing proxy-derived data (e.g., fixed SSTs) into the model because of the lack of interaction of the model components. Both approaches have deficiencies. The first ignores the potential for very different conditions in the past. The second raises issues of circularity in the experimental framework. In addition, the potential for an inconsistency between the ocean and atmospheric implied circulations is a fundamental challenge to uncoupled modeling techniques (Huber et al., 2001). Model simulations that do not treat atmosphere-ocean interaction or have a highly simplified atmosphere (or ocean) cannot adequately address the magnitude of the net surface energy and momentum fluxes because they do not properly represent changes in wind, temperature, precipitation fields, current structures, and modes of variability.

Although it has its own deficiencies, a fully coupled general circulation model (CGCM) permits us to avoid these pitfalls and provide a relatively independent model to compare climate proxy interpretations against. Fully coupled general circulation paleoclimate modeling is a new and rapidly evolving field, so it is important to understand the caveats. I discuss the difficulties and my methods in this paper, Huber and Sloan (2001), and Huber et al. (in press).

Most CGCMs require "flux corrections" to maintain a stable steady-state climate for modern conditions because of weaknesses in the model formulation. Without these corrections, the modeled climate drifts toward unrealistic values for important climate parameters. These models are not convergent on a realistic climate state even for perfectly known initial and boundary conditions and, consequently, cannot be used for paleoclimate modeling in the deep past. It is critical, therefore, to use a CGCM that does not require flux corrections for modern-day climate conditions when attempting to model the early Paleogene. The model used herein does not require flux corrections.

The model, the National Center for Atmospheric Research (NCAR) Climate System Model (CSM), is described below and by Boville and Gent (1998). The results presented here are produced with an updated version, 1.4, described for a modern and a Cretaceous experiment in Boville et al. (2001), Otto-Bliesner and Brady (2001), Otto-Bliesner et al. (2002), Large et al. (2001), and briefly below. The atmospheric and land models are Community Climate Model [CCM] 3.6 and Land Surface Model [LSM] 1.2 at T31 (~3.75° by 3.75°) resolution. These are coupled to NCAR's Ocean Model and the Community Sea Ice Model. The latter models are on a stretched grid with 0.9° equatorial and 1.8° high-latitude meridional grid spacing; zonal resolution is 3.6°. The ocean model is integrated with anisotropic horizontal viscosity (Large et al., 2001). As described in the references above, the major differences from CSM version 1 are (1) better-resolved tropical ocean circulations and thermocline structure and (2) improvements in conservation properties of flux coupler interpolation between component models.

It is not sufficient, however, to use a CGCM to model the early Paleogene ocean circulation; the model should be able to simulate tropical ocean circulations and tropical atmosphere-ocean interactions such as

the El Niño Southern Oscillation (ENSO). CSM version 1 has this capability (Large et al., 2001; Otto-Bliesner and Brady, 2001). Importantly, this version incorporates very small values of vertical diffusion and an implementation of anisotropic horizontal viscosity, providing excellent resolution of tropical current systems. The paleoposition determined during Leg 199 for the Paleogene suggests that it is the structure and properties of the thin (100–300 km), vigorous (100 cm/s), and variable eastward flowing North Equatorial Countercurrent (NECC) and North Subsurface Countercurrent (NSCC) that are likely to be critical.

Today the Pacific NECC and Equatorial Undercurrent (EUC) are, on average, vigorous eastward-flowing tropical currents, originating in the western Pacific warm pool, set up by pressure gradients associated with the across-Pacific thermocline tilt; the latitude of the NECC appears to be related to the Intertropical Convergence Zone (ITCZ) (Donguy and Meyers, 1996; Johnson et al., 2001, and references therein). These currents' magnitudes are tied to that of the Walker cell, which is related to the tilt of the thermocline (Rowe et al., 2000). The NSCC occurs at several hundred meters depth between 4° and 8° latitude and is linked to the 13°C thermostad in the eastern Pacific (Marin et al., 2000). As a consequence of their intimate ocean-atmosphere coupling, these currents change strength and depth extensively over the course of seasonal and ENSO cycles (Johnson et al., 2000). Overall, these currents usually provide a broad region of relatively fresh eastward flow at depths between 100 and 400 m, which I refer to as the NECC/NSCC complex. The dynamics of these currents were not well resolved in any previous Paleogene ocean-modeling investigation.

The details of the method developed to perform deep paleoclimate CGCM integrations are described in Huber and Sloan (2001). The topography and vegetation distributions used are described and extensively referenced in Sewall et al. (2000). Description of how the initial SST distributions were created can be found in Sloan et al. (2001). The creation of a bathymetric data set for the early Paleogene began with land-sea distributions created by Sewall et al. (2000), which were modifications to those described in Sloan and Rea (1996). Those land-sea distributions were then remapped from the $2° \times 2°$ distribution, described in Sewall et al. (2000), to the stretched grid of the ocean model. Isochron maps created by Royer et al. (1992) were then used to identify the paleolocations of Chron 25 and other late Paleocene–early Eocene isochrons in order to constrain the location of mid-ocean ridges during the early Paleogene. Further description of the creation of the bathymetry is found in Huber et al. (in press). The solar constant, orbital parameters, and all trace gas concentrations (excluding carbon dioxide) were set at preindustrial values.

Early Paleogene climate proxies that might be used as initial conditions for a modeling experiment are sparsely distributed in time and space, have inherent uncertainties associated with them, and may not constrain quantities that are important for climate modeling (e.g., salinity). There is also a good deal of uncertainty in boundary conditions, such as topographic or bathymetric reconstructions. I have preliminarily assessed the sensitivity of my spin-up method to uncertainty in bathymetry and initial conditions using an approach called "degradation" (covered in Huber and Sloan, 2001, and Huber et al., submitted) and demonstrated that there is little sensitivity to these features. Beginning with zonally constant ocean temperatures close to the proxy estimates of Zachos et al. (1994) for the early Eocene, the simulation has been integrated for over 3200 yr in the deep ocean with the accelerated, par-

tially asynchronous spin-up described in Huber and Sloan (2001). The simulation was then integrated in fully coupled mode for an additional 150 yr; averages over the last 50 yr are described herein. Trends in temperature and salinity were negligible (similar to values in Huber and Sloan, 2001). The tropical ocean properties produced in the simulation described here are nearly identical to those produced in the Huber and Sloan (2001) study despite the fact that the specified initial SST distributions were 4° cooler at low latitudes and 4° warmer at high latitudes, and deep ocean temperatures were 4° warmer than in the former study. This demonstrates that the modeling framework used here is robust.

RESULTS

NCAR's CSM has been used to simulate early Paleogene climate with realistic boundary conditions including 560 ppm pCO_2. At ~3500 m depth in the Pacific, temperatures are ~8°C, which is much warmer than modern values but in the cooler end of the range of values predicted from benthic foraminiferal calcite (closer to middle Eocene values). The meridional SST gradient within 30° of the equator is very similar to the modern value. The meridional SST gradient is much smaller than the modern one in the extratropical regions, which is consistent with the phenomenon of high-latitude amplification noted in many previous climate-change studies. Although the mean state of the simulation shows a strong Walker cell and associated warm pool (cold-tongue structure), the tropics do not collapse onto a steady La Niña or ENSO mode, and the ITCZ in the eastern Pacific is in approximately the same location as it is today.

To set up the context of this simulation, the annual average global upwelling distribution and Pacific Ocean current vectors at ~100 m depth are shown in Figure F1. There is clearly a large body of upwelled water in the eastern Pacific, and westward spanning tongues of upwelled water associated with the equator, the ITCZ in the Northern Hemisphere, and a probably spurious southern branch associated with a southern ITCZ. This latter feature is further discussed below. The current structure clearly reveals vigorous NECC and EUC currents as well as the larger-scale gyre structures throughout the Pacific (Fig. F1).

The net freshwater flux distribution is close to modern distributions; the locations of net precipitation (i.e., the ITCZ and warm pool and South Pacific Convergence Zone [SPCZ]) are at near-modern locations and magnitudes (top of Fig. F2). The seasonal cycle of net freshwater flux at 115°W (bottom of Fig. F2) is similar to that produced by the coupled models for modern day, as well as being close to observed values with the exception of a brief period (April–May) when the ITCZ is placed south of the equator.

In Figure F3, quantities are averaged through the upper 30 m of the model, which corresponds roughly to the Ekman layer and the mixed-layer depth. In Figure F3A, annual average temperature, salinity, and currents in this layer are shown. There is a large east-west gradient in Ekman layer temperature (7°C) along the equator, and the warm pool is displaced southward in the west. A tongue of warm (30°C) water is displaced north of the equator in the east. Salinity gradients are predominately zonal (east-west), and low salinity values are largely associated with the precipitation in the warm pool. The currents in this layer are very similar to those observed today and are quite vigorous (~30 cm/s).

F1. Global land-sea distribution and annual-average map of upwelling into the thermocline, p. 14.

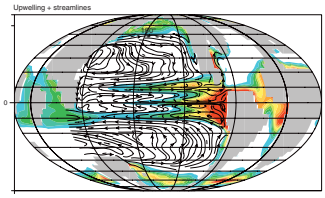

F2. Net freshwater flux in centimeters and the seasonal cycle at 115°W, p. 15.

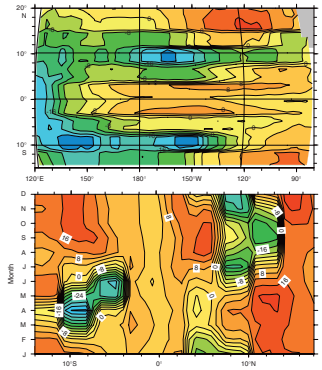

F3. Quantities averaged through the upper 30 m of the model, p. 16.

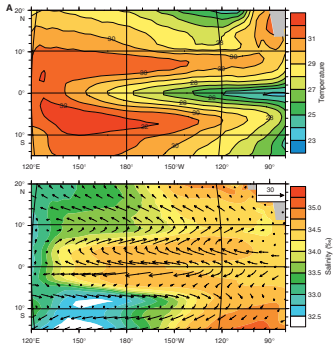

Because of current and upwelling variability over the seasonal cycle, there is an impressive degree of seasonal variation in temperature, salinity, and flow streamlines, despite the fact that the tropics are sometimes considered homogenous (e.g., Barron, 1995). I will mostly discuss and contrast the seasonal extremes which in the tropics are approximately April-May-June (AMJ) and October-November-December (OND). In AMJ, the western Pacific warm pool is at its extreme in terms of temperature and southward displacement and there is substantial cross-equatorial transport in both the east and west Pacific in the Ekman layer (Fig. **F3B**). During OND, flow is much more zonal and vigorous (Fig. **F3**), and upwelling of cold water in the eastern Pacific and a Northern Hemisphere ITCZ is best developed (Fig. **F3C**).

In Figure **F3D,** annual average upwelling, streamlines of the flow, and an estimate of seawater $\delta^{18}O$ (hereafter δ_w) are plotted. The δ_w distribution in Figure **F3D** is calculated from the empirical relation between seawater salinity and δ_w proposed by Fairbanks et al. (1997) for the equatorial region. Fortunately, this modern correlation is (1) excellent ($R^2 = 0.92$), (2) was developed for this specific region, and (3) is accurate for the kind of variations in temperature and precipitation that occur in this region over ENSO cycles. In keeping with the model-produced salinity distribution, the calculated δ_w shows little meridional variation; therefore, there should be little need to correct for δ_w variations along the tropical transect when foraminiferal oxygen isotope ratios derived from Leg 199 are eventually processed (provided suitable foraminifers are found).

The streamlines in Figure **F3D** highlight the overall current structure (de-emphasizing the current strength) and show the correspondence between gyres and expected upwelling (both are a result of the Ekman transport divergence). The mean annual depth of the 24°C isotherm, which corresponds to the mid- to upper thermocline in this simulation, shows the same east-west tilt characteristic of the present and a similar seasonal cycle of this quantity as produced in a modern-day simulation along the equator (Fig. **F3E, F3F, F3G**). The relationship between the thermocline distribution and the upwelling distribution is clear, and thermocline depth can therefore be considered an indicator in the simulation of upwelling changes as well (Fig. **F3E, F3F, F3G**).

Since this simulation is meant to be a straw man, I have made a prediction of the $\delta^{18}O$ ratio that should be expected from two different depth levels, mixed-layer dwellers (top of Fig. **F3H**), and above-thermocline dwellers (bottom of Fig. **F3H**) based on these model results (hereafter δ_c). To do this, I used the calculated δ_w and model-predicted temperatures and inverted the Bemis et al. (1998) temperature ($\delta_c - \delta_w$) to produce an estimated relation for δ_c (in a manner similar to Schmidt, 1999). I chose the Bemis et al. (1998) equation as the estimator for two reasons. Most importantly, this relation produces the same results as the commonly used Erez and Luz (1983) relationship within this temperature range, so my results are directly comparable to previous proxy data studies. Secondly, because the relationship is linear and has the same slope as their equation, it is simple to immediately assess the possible effects of different light levels (and possibly alkalinity) and depth habits by subtracting 0.333 from the values here. It is clear that the predicted values show substantial structure and variability, which remain to be tested against data. Importantly, these results indicate that the vast majority of the signal recorded by foraminiferal δ_c in this region is due to temperature variations and not salinity (δ_w) variations. Addition-

ally, depth habit will be a crucial factor to constrain, as it generates variations in predicted δ_c of over 1.0‰. More details on that issue follow in the discussion of the meridional transects.

As shown in the annual averages in Figure F4A, at a mean depth of ~100 m, upwelling in the east is associated with cool temperatures and the downward-dipping thermocline in the west (Fig. F3G) is associated with warm temperatures. At this level, the EUC is still quite vigorous (20 cm/s). Over the seasonal cycle, there are large changes in the magnitude of the EUC and NECC/NSCC complex (Fig. F4B, F4C).

In the region below the upper thermocline (190–550 m), where the seasonal cycle is less evident (not shown), the tracer properties are relatively homogenous (12°C; 34.6 ppt), but the current shows interesting structure (Fig. F5). The presence of a deep NECC dominates the deep tropics and is responsible for transport water from the western Pacific north and eastward at 3 cm/s. This pattern is pronounced in deeper waters (900–2000 m) (Fig. F6), where variations in temperature and salinity are due to the deep and vigorous (1 cm/s) NECC.

In keeping with the straw man approach, specific predictions are presented in Figure F7 to be tested against the results of Leg 199. This figure presents a transect along 115°W from 15°S to 20°N of the seasonal extremes of east-west (zonal) velocity and temperature and my estimate of δ_c. Upwelling clearly plays an important role within 4° of the equator. Similarly, the importance of zonal advection of plankton and water mass properties from the warm pool or from the Atlantic must not be neglected. As this figure shows, the currents are extremely vigorous and variable. Again, it should be noted that the structure of the results south of ~5°S is probably spurious given the fact this model (and all CGCMs) produce a spurious Southern Hemisphere ITCZ. This makes it likely that the currents and water mass properties in that region are not correct in the simulations of the past. Not clearly visible on Figure F7 is that fact that benthic conditions at 115°W may reflect input of a "young" Atlantic water mass entering into tropical current systems via the Panamanian Seaway (Huber and Sloan, 2001; Huber et al., submitted).

DISCUSSION AND SUMMARY

The properties predicted by this simulation are probably incorrect in a number of respects, but this section will not be used to hedge and stipulate because that would be counter to the goal of having a straw man. It is where the model and data meaningfully disagree that the most new information will be learned. I will discuss the most likely weaknesses and strengths of the model and some ways in which the model predictions might be compared productively with the climate proxies and the arguments embodied in the Leg 199 drilling proposal and the "Leg 199 Scientific Prospectus."

The most important weakness of this model and all CGCMs is the tendency to have a split ITCZ, that is, an overly strong Southern Hemisphere ITCZ in the central and eastern Pacific. In the modern day, the Northern Hemisphere preference of the ITCZ leads to a cross-equatorial asymmetry in flow and water mass properties, with a strong NECC but no substantial SECC in the eastern Pacific. The atmospheric GCM used in this study accurately reproduces the ITCZ position and seasonal movement when driven by modern SSTs. It has been proposed that the bias in the coupled simulation is due to some error in the feedback be-

F4. Annual average temperature for the thermocline layer, p. 24.

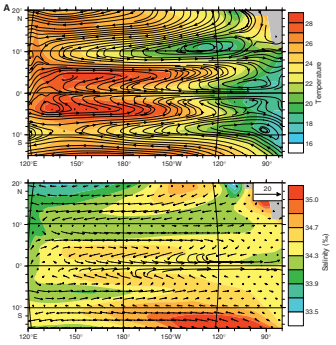

F5. Temperature, streamlines, salinity, and current vectors for 190–550 m, p. 27.

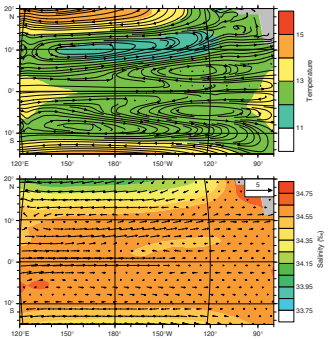

F6. Temperature, streamlines, salinity, and current vectors for 900–2000 m, p. 28.

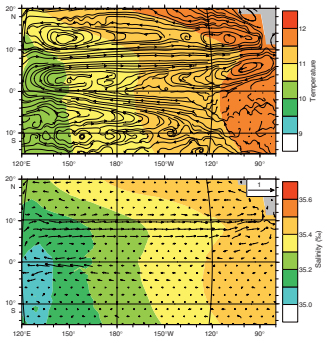

tween the ocean currents, upwelling, stratus clouds, and wind fields in the eastern Pacific (more below).

This brings us to an important point, with regard to both the deficiency of CGCMS in modeling the eastern Pacific ITCZ and an underlying assumption in the Leg 199 drilling proposal. The theory, widely used in the Leg 199 drilling proposal and the "Leg 199 Scientific Prospectus," postulates that the Northern Hemisphere preference for the ITCZ is due to the larger land area in the Northern Hemisphere, which drags the "thermal equator" across the geographic equator (espoused originally by Flohn, 1981). The theory that the ITCZ responds to hemisphere-wide land-sea fraction differences is not currently accepted by the climate community and may not be the best conceptual model for paleoclimate investigations either.

In fact, there is no general theory that is completely successful in explaining the location of the ITCZ. Current work on this subject, exemplified by "Why is the ITCZ Mostly North of the Equator" (Philander et al., 1996), takes into account the fact that the Northern Hemisphere preference for the ITCZ is a regional feature (i.e., in the eastern Pacific and Atlantic) and caused by regional features. For example, the western Pacific warm pool and the largely ignored South Pacific Convergence Zone do not have a Northern Hemisphere preference. Thus, the key question is, "What sets the location of the ITCZ in the eastern Pacific?"

Although no full explanation currently exists, the orientation of the coast of South and Central America with respect to the western Pacific warm pool appears to be very important because of the impact of feedback involving near-coastal wind-driven upwelling and downwelling. As summarized in Thuburn and Sutton (2000), the asymmetries thus created are enhanced by and, in turn, enhance the regional warming of the ocean north of the equator and ocean cooling south of the equator. Some role for the Central American summer monsoon has also been suggested (Mitchell and Wallace, 1992). Stratus cloud albedo feedback further enhances the cross-equatorial temperature gradient and associated large-scale circulation patterns. Because of the complexity of the feedback and the fact that we still do not have a full theory for the ITCZ, CGCMs do not reproduce the seasonal cycle of the ITCZ in the eastern Pacific correctly. These factors are just as likely to have controlled the eastern Pacific ITCZ behavior in the past as they do today. Indeed, there is support for such linkages already in the early Neogene record (Tsuchi, 1997). Hopefully, a major contribution of Leg 199 will be in increasing our understanding of these ITCZ processes, but that requires dealing with all of the possible factors involved.

In a related vein, although frequent attempts have been made, there is some difficulty in attributing a special relationship between the location of the ITCZ and a sediment bulge. This difficulty becomes especially apparent when trying to make specific predictions about the proxy record from a quantitative climate model, as I do in Figure **F7.** Clearly, there are many aspects of productivity and accumulation and their relationship to ocean circulation that are still poorly understood (e.g., Ragueneau et al., 2000; Friedrichs and Hofmann, 2001), and these present practical difficulties but also exciting opportunities for Leg 199 researchers. However, there are specific questions about variations in accumulation rates in the Pacific that may need to be considered. Today there is enhanced sedimentation at the equator in the western Pacific warm pool (Higgins et al., 1999; Broecker et al., 1999), which is very poorly understood, and it raises questions about our understanding, in general, of the mechanisms that might focus (or unfocus) sediment in

F7. Meridional transects along 115°W, p. 29.

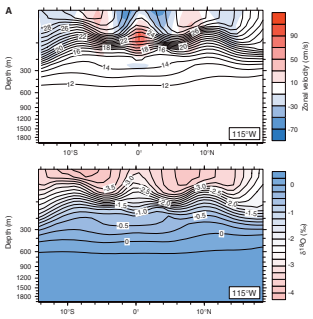

the equatorial Pacific, even in the absence of an ITCZ. Furthermore, the presence of enhanced accumulation rates at the equator in the western and central Pacific during much of the Cretaceous (Ogg et al., 1992) (another extreme "greenhouse" climate interval) is difficult to reconcile with the conceptual picture laid out in the Leg 199 drilling proposal and the "Leg 199 Scientific Prospectus." It should also be remembered that the warm pool is also a region of productivity and upwelling (although the upwelling arrives at a deeper level [Helber and Weisberg, 2001]).

In general, the model results do not predict dramatic changes in the major features of the tropical ocean or atmosphere circulation in equilibrium with realistic early Paleogene conditions. It should also be acknowledged that the winter-season extratropical continental temperatures are colder than terrestrial proxies, so the simulation does not reproduce "equable climates." Other model results indicate ~2000 ppm pCO_2 would be required to produce equable climates, although mean tropical SSTs would then be at or above 34°C (C.J. Shellito, L.C. Sloan, and M. Huber, unpubl. data).

The fact that simulated equator-to-pole and surface-to-deep temperature gradients are substantially less than modern gradients has little impact on the results shown here because the tropical thermocline, ITCZ precipitation, and tropical wind fields are all controlled by the tropical–subtropical temperature gradient (Huber and Sloan, 2000). The tropical–subtropical meridional temperature gradient produced by the simulation is very close to modern (e.g., Huber and Sloan, 2001). There are, however, many important regional features of the eastern Pacific that would have been difficult to predict without the modeling framework used in this study. According to the model, the mean location of the ITCZ should be in about the same place as today, as should the major upwelling regions. The seasonal cycles of temperature, precipitation, and current variations are similar to those simulated for today but with potentially important second-order differences, including somewhat broader seasonal swings of these characteristics (~3° of latitude) and a stronger Walker cell. Thus, on a seasonal basis, the region of upwelling (and productivity?) is broader than in modern cases. If major differences are found between the model results presented here and the results of Legs 198 and 199, a unique opportunity might present itself for understanding the failure of the model with regards to both key climatic features.

It bears mentioning that the response of tropical circulations in CGCMs to increased greenhouse gas concentrations (in modern-day simulations) is still very sensitive to details of model parameterizations. There is currently a significant debate as to whether or not increased greenhouse-gas concentrations should lead to a mean state in the tropics that bears more of a resemblance to La Niña or ENSO conditions or whether there should be no change in the mean state at all (Cane et al., 1997; Timmerman et al., 1999; Fedorov and Philander, 2000; Jin et al., 2001). Although the simulation presented here produces a tropical system that is similar to the modern system, it is slightly skewed toward a permanent La Niña state. If the "correct" state is more skewed toward a permanent ENSO state, as has been suggested by Sun (2000), Liu and Huang (1997), and Fedorov and Philander (2000), the difference may be noticeable in the Leg 199 results. The notable difference, according to Sun (2000), Liu and Huang (1997), and Fedorov and Philander (2000), is that the eastern equatorial upwelling zone should not exist in past

warm climates. Instead, it should be replaced by a broad, warm, and well-stratified region more similar to the warm pool of today.

If data from Leg 198 and 199 can either confirm or rule out the presence of a warm-pool cold-tongue (downwelling-upwelling) dichotomy pattern in the Pacific, the impact on controversies in modern and future climate change theories will be substantial. Romero et al. (2001) present clear evidence from the early 1990s that ENSO largely controls the temporal and spatial variability in export production in parts of the Pacific, with up to 75% decreases in production during ENSO events and a tendency for diatoms to be much more sensitive to such fluctuations than radiolarians. On the face of things, it appears that the pattern of extreme radiolarian productivity in the East Pacific (found during Leg 199) is in keeping with the model results presented here, contrary to prediction that there should be no thermocline tilt and much reduced upwelling in past warm climates.

ACKNOWLEDGMENTS

The author gratefully acknowledges his Ph.D. supervisor L.C. Sloan for mentorship and support via National Science Foundation (NSF) grant ATM9810799 and the D. and L. Packard Foundation as well as the support of Gary Shaffer and the Danish Center for Earth System Science. Discussions with E. Brady, R. Caballero, M. Lyle, J.C. McWilliams, T. Moore, B. Otto-Bliesner, P. Pearson, D. Rea, and J. Zachos were welcome and informative. The CSM model, computer time, and graphics tools (NCL) were provided through NCAR by NSF, for which I am grateful.

REFERENCES

Barron, E.J., 1987. Eocene equator-to-pole surface ocean temperatures: a significant climate problem? *Paleoceanography,* 2:729–739.

Barron, E., Tropical climate stability and implications for the distribution of life, 1995. *In Effects of Past Global Change on Life:* Washington, D.C. (National Academy Press).

Bemis, B.E., Spero, H.J., Bijma, J., and Lea, D.W., 1998. Reevaluation of the oxygen isotopic composition of planktonic foraminifera: experimental results and revised paleotemperature equations. *Paleoceanography,* 13:150–160.

Boville, B.A., and Gent, P.R., 1998. The NCAR Climate System Model Version One. *J. Clim.,*11:1115–1130.

Boville, B.A., Kiehl, J.T., Rasch, P.J., and Bryan, F.O., 2001. Improvements to the NCAR CSM-1 for transient climate simulations. *J. Clim.,* 14:164–179.

Bralower, T.J., Zachos, J.C., Thomas, E., Parrow, M., Paull, C.K., Kelly, D.C., Premoli Silva, I., Sliter, W.V., and Lohmann, K.C., 1995. Late Paleocene to Eocene paleoceanography of the equatorial Pacific Ocean: stable isotopes recorded at Ocean Drilling Program Site 865, Allison Guyot. *Paleoceanography,* 10:841–865.

Broecker, W.S., Clark, E., McCorkle, C.D., Hajdas, I., and Bonani, G., 1999. Coretop C^{14} ages as a function of latitude and water depth on the Ontong-Java Plateau, *Paleoceanography,* 14:13–22.

Cane, M.A., Clement, A.C., Kaplan, A., Kushnir, Y., Pozdnyakov, D., Seager, R., Zebiak, S.E., and Murtugudde, R., 1997. Twentieth-Century sea surface temperature trends. *Science,* 275:957–960.

Crowley, T.J., and Zachos, J.C., 2000. Comparison of zonal temperature profiles for past warm time periods. *In* Huber, B.T., MacLeod, K.G., and Wing, S.L. (Eds.), *Warm Climates in Earth History:* Cambridge (Cambridge Univ. Press), 79–131.

DeConto, R.M., Thompson, S.L., and Pollard, D., 2000. Recent advances in paleoclimate modeling: toward better simulations of warm paleoclimates. *In* Huber, B.T., MacLeod, K.G., and Wing, S.L. (Eds.), *Warm Climates in Earth History:* Cambridge (Cambridge Univ. Press), 21–49.

Donguy, J.R., and Meyers, G., 1996. Mean annual variation of transport of major currents in the tropical Pacific Ocean. *Deep-Sea Res.,* 43:1105–1122.

Erez, J., and Luz, B., 1983. Experimental paleotemperature equation for planktonic foraminifera. *Geochim. Cosmochim. Acta,* 47:1025–1031.

Fairbanks, R.G., Evans, M.N., Rubenstone, J.L., Mortlock, R.A., Broad, K., Moored, M.D., and Charles, C.D., 1997. Evaluating climate indices and their geochemical proxies measured in corals. *Coral Reefs,* 16:93–100.

Fedorov, A.V., and Philander, S.G., 2000. Is El Niño changing? *Science,* 288:1997–2002.

Flohn, H., 1981. A hemispheric circulation asymmetry during late Tertiary. *Geol. Rundsch.,* 70:725–736.

Friedrichs, M.A.M., and Hofmann, E.E., 2001. Physical control of biological processes in the central equatorial Pacific Ocean, *Deep-Sea Res,* 48:1023–1069.

Greenwood, D.R., and Wing, S.L., 1995. Eocene continental climates and latitudinal temperature gradients. *Geology,* 23:1044–1048.

Helber, R.W., and Weisberg, R.H., 2001. Equatorial upwelling in the western Pacific warm pool. *J. Geophys. Res.,* 106:8989–9004.

Higgins, S.M., Broecker, W., Anderson, R., McCorkle, D.C., and Timothy, D., 1999. Enhanced sedimentation along the Equator in the western Pacific, *Geophys. Res. Lett.,* 23:3489–3492.

Huber, M., and Sloan, L.C., 2000. Climatic response to tropical sea surface temperature changes on a "greenhouse" Earth. *Paleoceanography,* 15:443–450.

Huber, M., and Sloan, L.C., 2001. Heat transport, deep waters, and thermal gradients: coupled simulation of an Eocene "greenhouse" climate. *Geophys. Res. Lett.,* 28:3481–3484.

Huber, M., Sloan, L.C., and C. Shellito, in press. Early Paleogene oceans and climate: A fully coupled modelling approach using the NCAR CSM, *Early Paleogene Climate GSA Special Volume*.

Jin, F.F., Hu, Z.Z., Latif, M., Bengtsson, L., and Roeckner, E., 2001. Dynamical and cloud-radiation feedbacks in El Niño and greenhouse warming. *Geophy. Res. Lett.,* 28:1539–1542.

Johnson, G.C., McPhaden, M.J., Rowe, G.D., and McTaggart, K.E., 2000. Upper equatorial Pacific Ocean current and salinity variability during the 1996/1998 El Niño-La Niña cycle. *J. Geophys. Res.* 105:1037–1053.

Johnson, G.C., McPhaden, M.J., and Firing, E., 2001. Equatorial Pacific Ocean horizontal velocity, divergence, and upwelling. *J. Phys. Oceanogr.,* 31:839–849.

Large, W.G., Danabasoglu, D., McWilliams, J.C., Gent, P.R., and Bryan, F.O., 2001. Equatorial circulation of a global ocean climate model with anisotropic horizontal viscosity. *J. Phys. Oceanogr.,* 31:518–536.

Liu, Z.Y., and Huang, B., 1997. A coupled theory of tropical climatology: warm pool, cold tongue, and Walker Circulation. *J. Clim.,* 10:1662–1679.

Marin, F., Hua, B.L., and Wacongne, S., 2000. The equatorial thermostad and subsurface countercurrents in light of the dynamics of atmospheric Hadley cells. *J. Mar. Res.,* 58:405–437.

Mitchell, T.P., and Wallace, J.M., 1992. The annual cycle in equatorial convection and sea-surface temperature. *J. Clim.,* 10:1140-1156.

Ogg, J.G., Karl, S.M., and Behl, R.J., 1992. Jurassic through Early Cretaceous sedimentation history of the central equatorial Pacific and of Sites 800 and 801. *In* Larson, R.L., Lancelot, Y., et al., *Proc. ODP, Sci. Results,* 129: College Station, TX (Ocean Drilling Program), 571–613.

Otto-Bliesner, B.L., and Brady, E.C., 2001. Tropical Pacific variability in the NCAR climate system model. *J. Clim.,* 14:3587–3607.

Otto-Bliesner, B.L., Brady, E.C., and Shields, C., 2002. Late Cretaceous ocean: coupled simulations with the National Center for Atmopsheric Research Climate System Model. *J. Geophys. Res.*, 107:10.1029/2001JD000821.

Pearson, P.N., Ditchfield, P.W., Singano, J., Harcourt-Brown, K.G., Nicholas, C.J., Olsson, R.K., Shackleton, N.J., and Hall, M.A., 2001. Warm tropical sea surface temperatures in the Late Cretaceous and Eocene epochs. *Nature,* 413:481–487.

Philander, S.G.H., Gu, D., Halpern, D., Lambert, G., Lau, N.C., Li, T., and Pacanowski, R.C., 1996. Why the ITCZ is mostly north of the Equator, *J. Clim.,* 9:2958–2972.

Ragueneau, O., Tréguer, P., Leynaert, A., Anderson, R.F., Brzezinski, M.A., DeMaster, D.J., Dugdale, R.C., Dymond, J., Fischer, G., Francois, R., Heinze, C., Maier-Reimer, E., Martin-Jézéquel, V., Nelson, D.M., and Quéguiner, B., 2000. A review of the Si cycle in the modern ocean: recent progress and missing gaps in the application of biogenic ipal as a paleoproductivity proxy. *Global Planet. Change,* 26:317–365.

Romero, O.E., Hebbeln, D., and Wefer, G., 2001. Temporal and spatial variability in export production in the SE Pacific Ocean: evidence from siliceous plankton fluxes and surface sediment assemblages. *Deep-Sea Res.,* 48:2673–2697.

Rowe, G.D., Firing, E., and Johnson, G.C., 2000. Pacific equatorial subsurface countercurrent velocity, transport, and potential vorticity. *J. Phys. Oceanogr.,* 30:1172–1187.

Royer, J.Y., 1992. *A global isochron chart,* University of Texas Institute for Geophysics, Technical Report No. 117.

Schmidt, G.A., 1999. Forward modeling of carbonate proxy data from planktonic foraminfera using oxygen isotope tracers in a global ocean model. *Paleoceanography,* 14:482–497.

Schrag, D.P., 1999. Effects of diagenesis on the isotopic record of late Paleogene tropical sea surface temperatures. *Chem. Geol.,* 161:215–224.

Sewall, J.O., Sloan, L.C., Huber, M., and Wing, S., 2000. Climate sensitivity to changes in land surface characteristics. *Global Planet. Change,* 26:445–465.

Sloan, L.C., and Barron, E.J., 1990. *Equable* climates during Earth history. *Geology,* 18:489–492.

Sloan, L.C., Huber, M., Crowley, T.J., Sewall, J.O., and Baum, S., 2001. Effect of sea surface temperature configuration on model simulations of "equable" climate in the Early Eocene. *Palaeogeogr. Palaeoclimatol. Palaeoecol.*, 167:321-335.

Sloan, L.C., and Rea, D.K., 1996. Atmospheric CO_2 of the early Eocene: a general circulation modeling sensitivity study, *Palaeogeogr. Palaeoclimatol. Palaeoecol.,* 119:275–292.

Sun, D.Z., 2000. Global climate change and El Niño: A theoretical framework, *In* Diaz H.F. and Markgraf, V. (Eds.), *El Niño and the Southern Oscillation:* (Cambridge University Press), 443-463.

Thuburn, J., and Sutton, R.T., 2000. The seasonal cycle of tropical Pacific sea surface temperature in a coupled GCM. *Climate Dynamics,* 16:935–947.

Timmerman, A., Oberhuber, J., Bacher, A., Esch, M., Latif, M., and Roeckner, E., 1999. Increased El Niño frequency in a climate model forced by future greenhouse warming. *Nature,* 398:694–697.

Tsuchi, R., 1997. Marine climatic responses to Neogene tectonics of the Pacific Ocean seaways. *Tectonophysics,* 281:113–124.

Wolfe, J.A., 1994. Tertiary climatic changes at middle latitudes of western North America. *Palaeogeogr., Palaeoclimatol., Palaeoecol.,* 108:195–205.

Zachos, J.C., Stott, L.D., and Lohmann, K.C., 1994. Evolution of early Cenozoic marine temperatures. *Paleoceanography,* 9:353–387.

Figure F1. Global land-sea distribution and annual average map of upwelling into the thermocline. Red = regions of vigorous upwelling, green to blue = regions of weak upwelling, white = areas of mean downwelling. Current streamlines at ~100 m are shown for the Pacific. All map views are projected on a Mollweide projection.

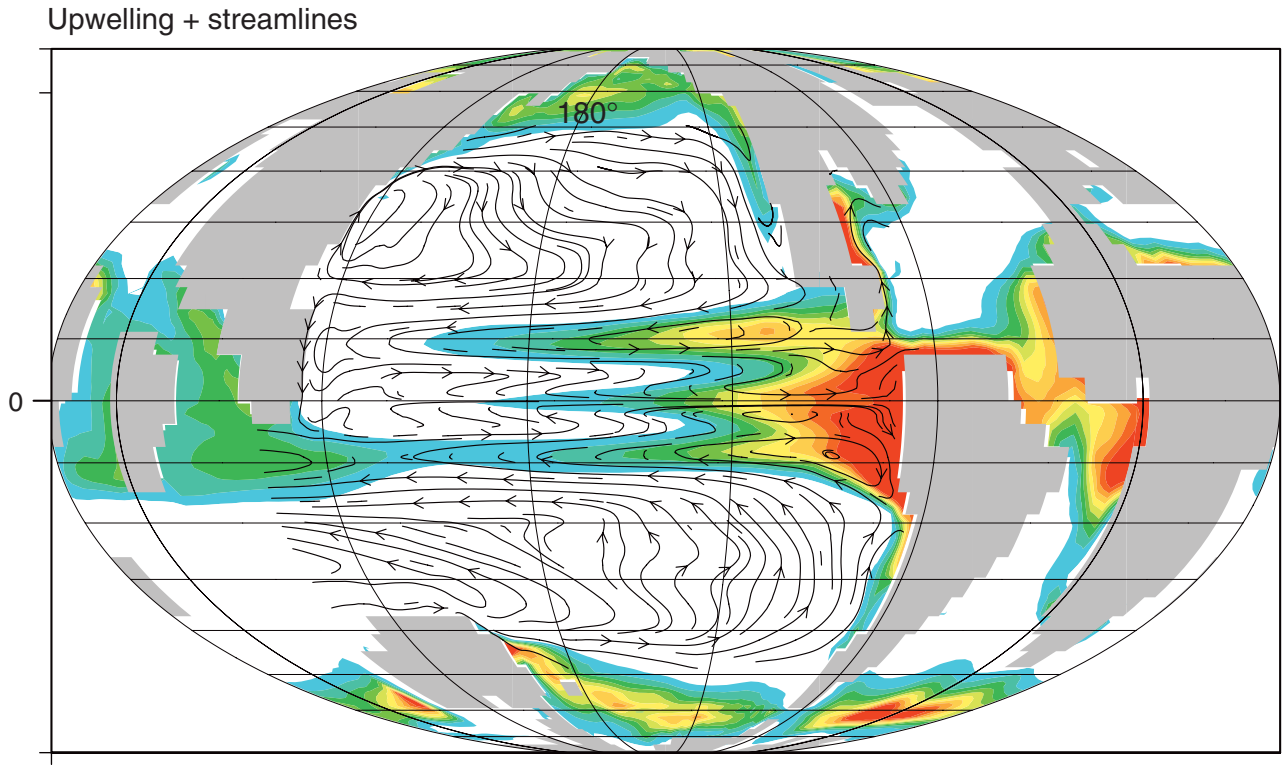

Figure F2. Net freshwater flux (centimeters per month) (top) and the seasonal cycle at 115°W (bottom).

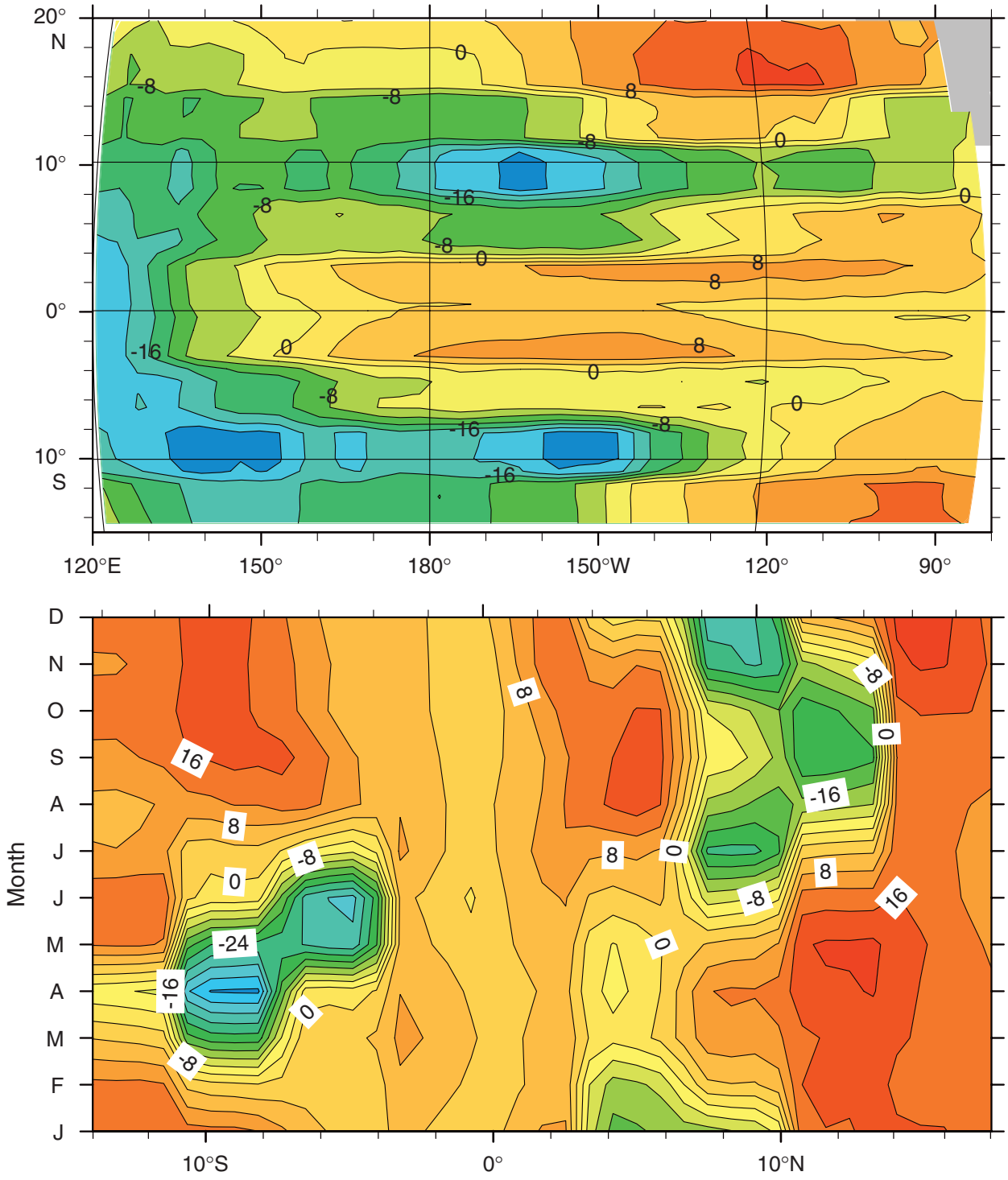

Figure F3. Quantities averaged through the upper 30 m of the model, which correspond roughly to the Ekman layer and the mixed layer depth (with exceptions as noted below). **A.** Annual average temperature (top) and salinity and current vectors (centimeters per second) (bottom) in this layer. (Continued on next seven pages.)

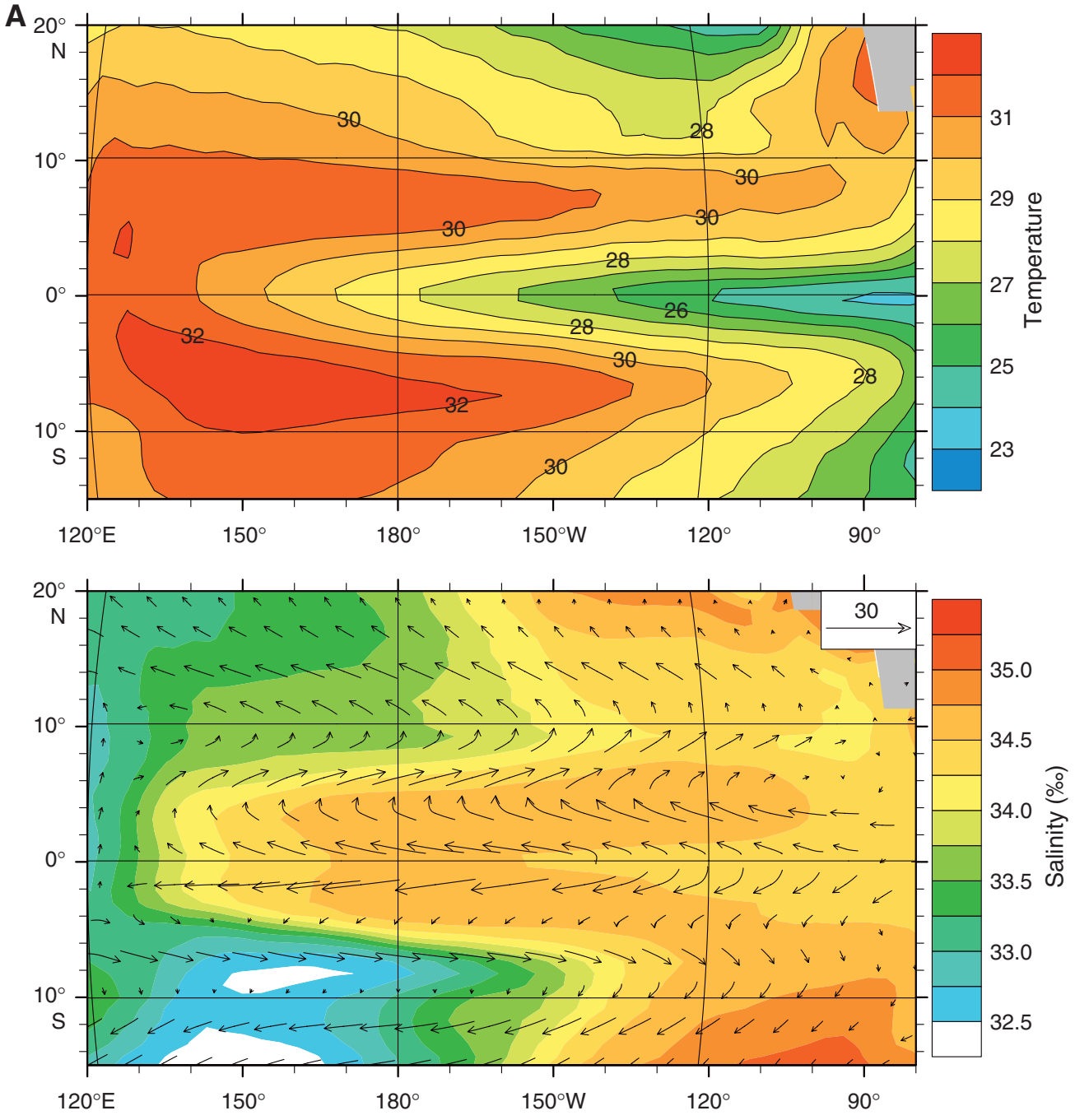

Figure F3 (continued). B. AMJ average temperature and streamlines (top) and AMJ salinity and current vectors (centimeters per second) (bottom) in the Ekman Layer (upper 30 m).

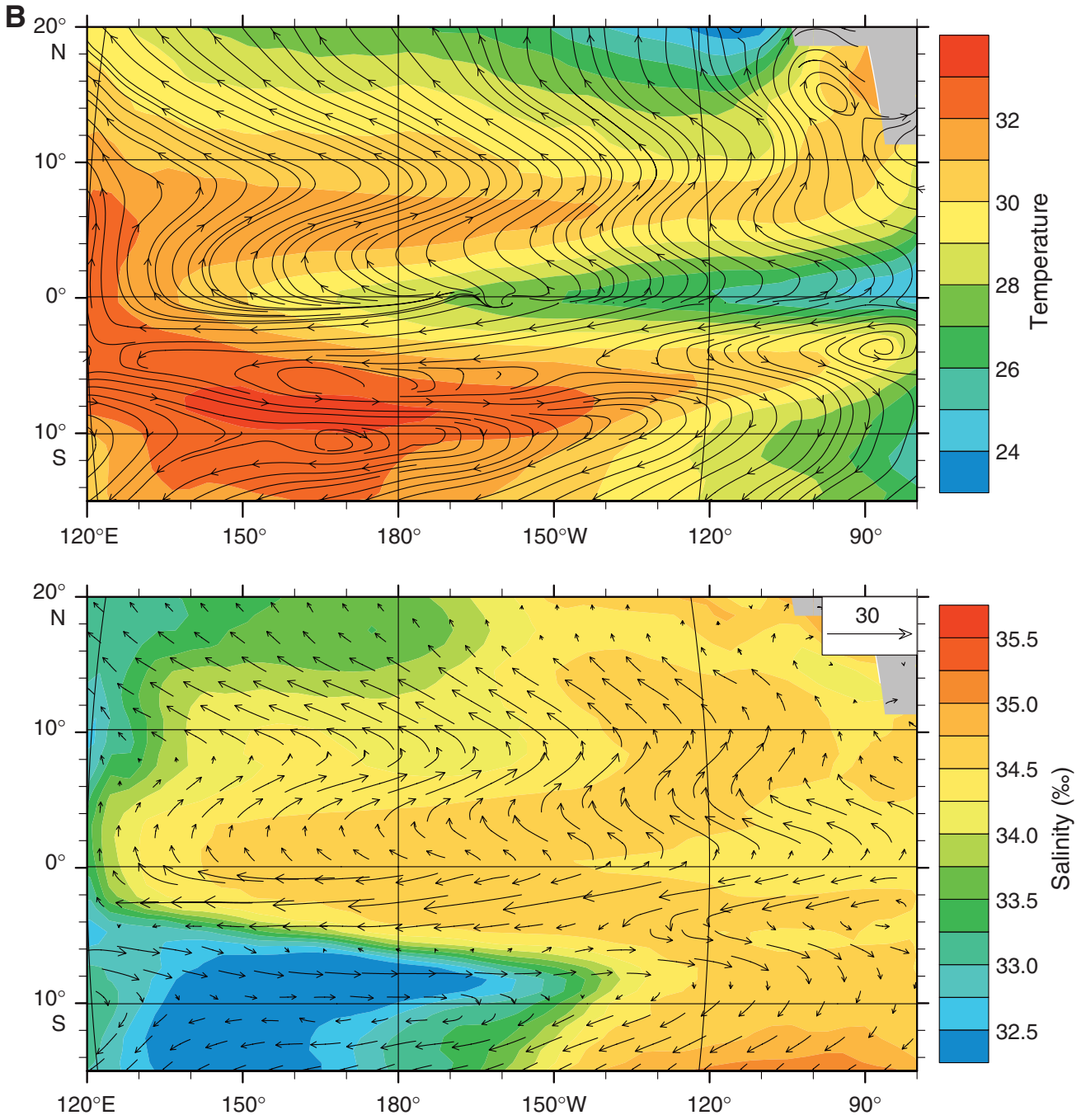

Figure F3 (continued). C. OMD average temperature and streamlines (top) and OMD salinity and current vectors (centimeters per second) (bottom) in the Ekman Layer (upper 30 m).

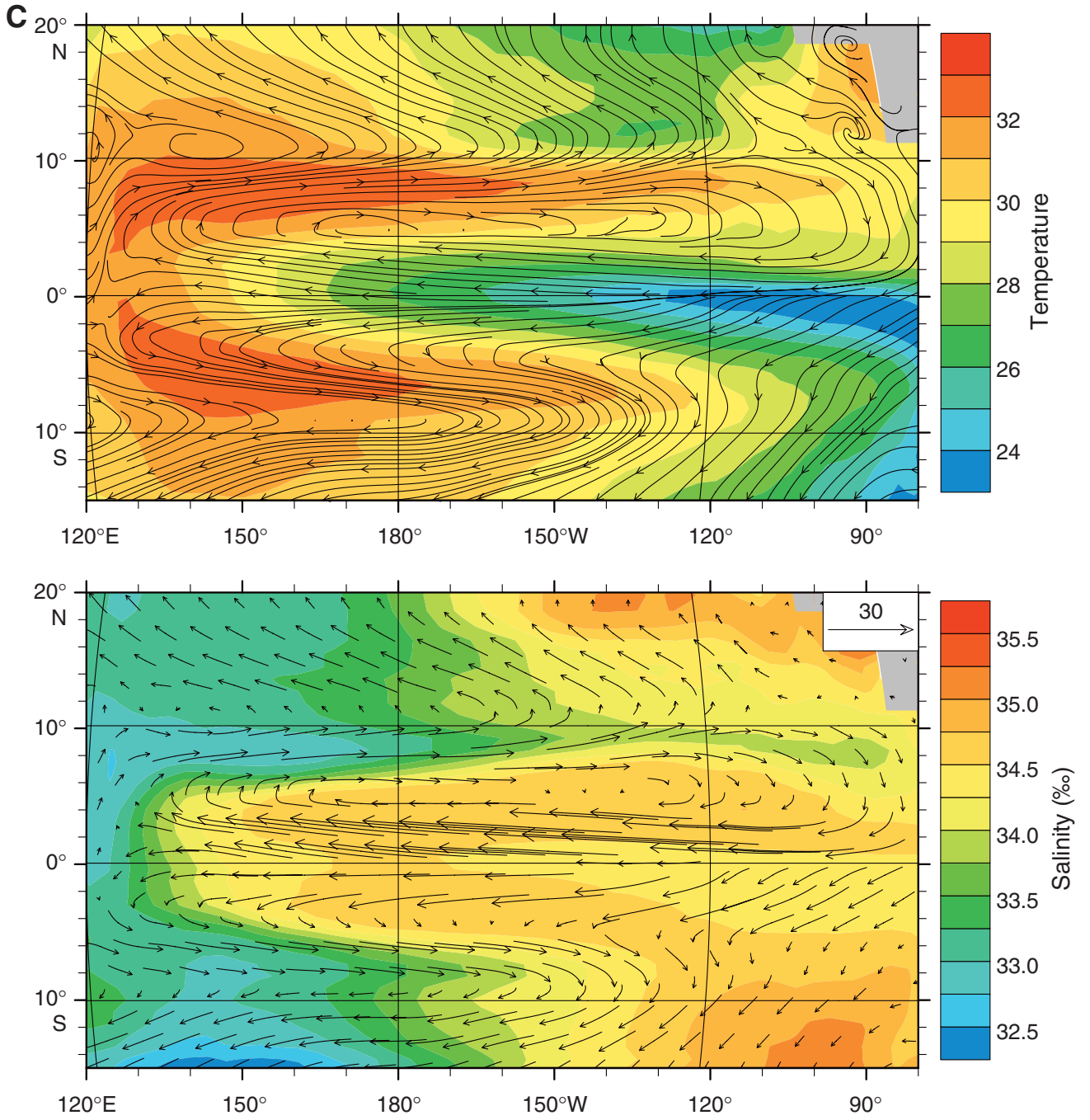

Figure F3 (continued). D. Annually averaged upwelling into the upper 30 m (Ekman Layer) (top) and streamlines (bottom) are shown. Green to blue = regions of weak upwelling, white = areas of mean downwelling. Estimated seawater $\delta_{18}O‰$ VMSO (Fairbanks et al., 1997)

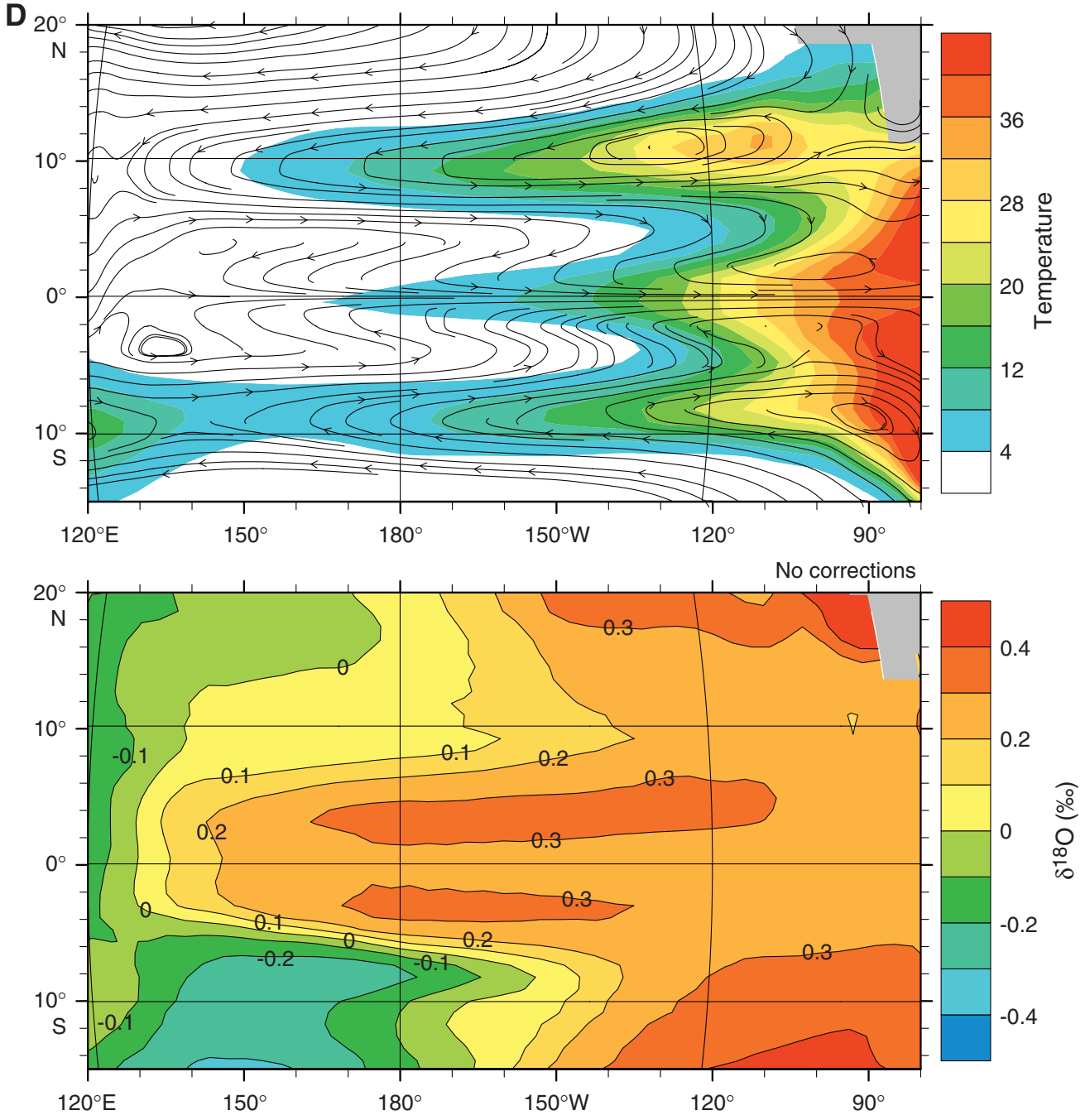

Figure F3 (continued). E. The mean annual depth (24°C isotherm) (top) and seasonal cycle of the thermocline (bottom).

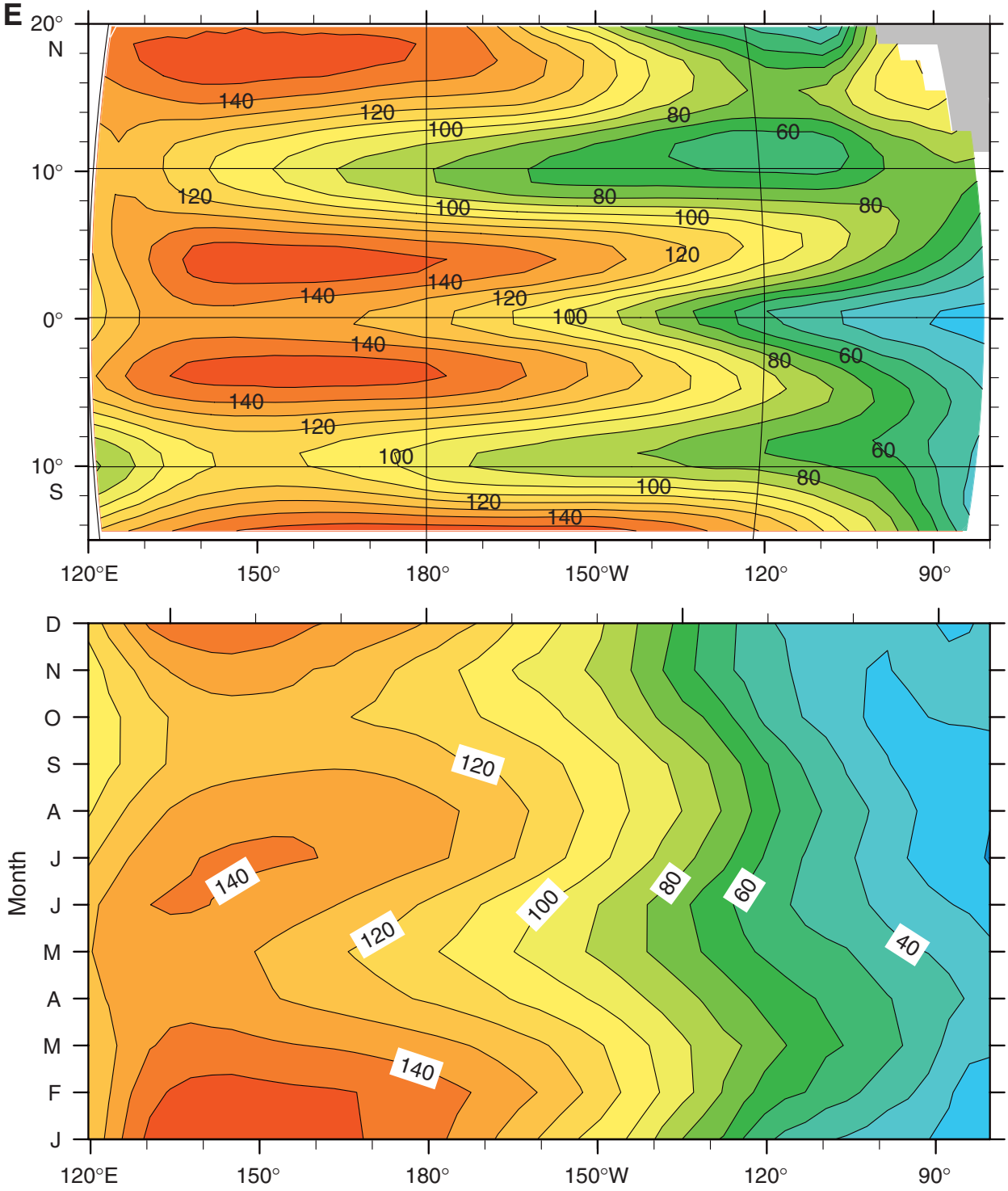

Figure F3 (continued). **F.** Thermocline depth of the 24°C isotherm at 115°W.

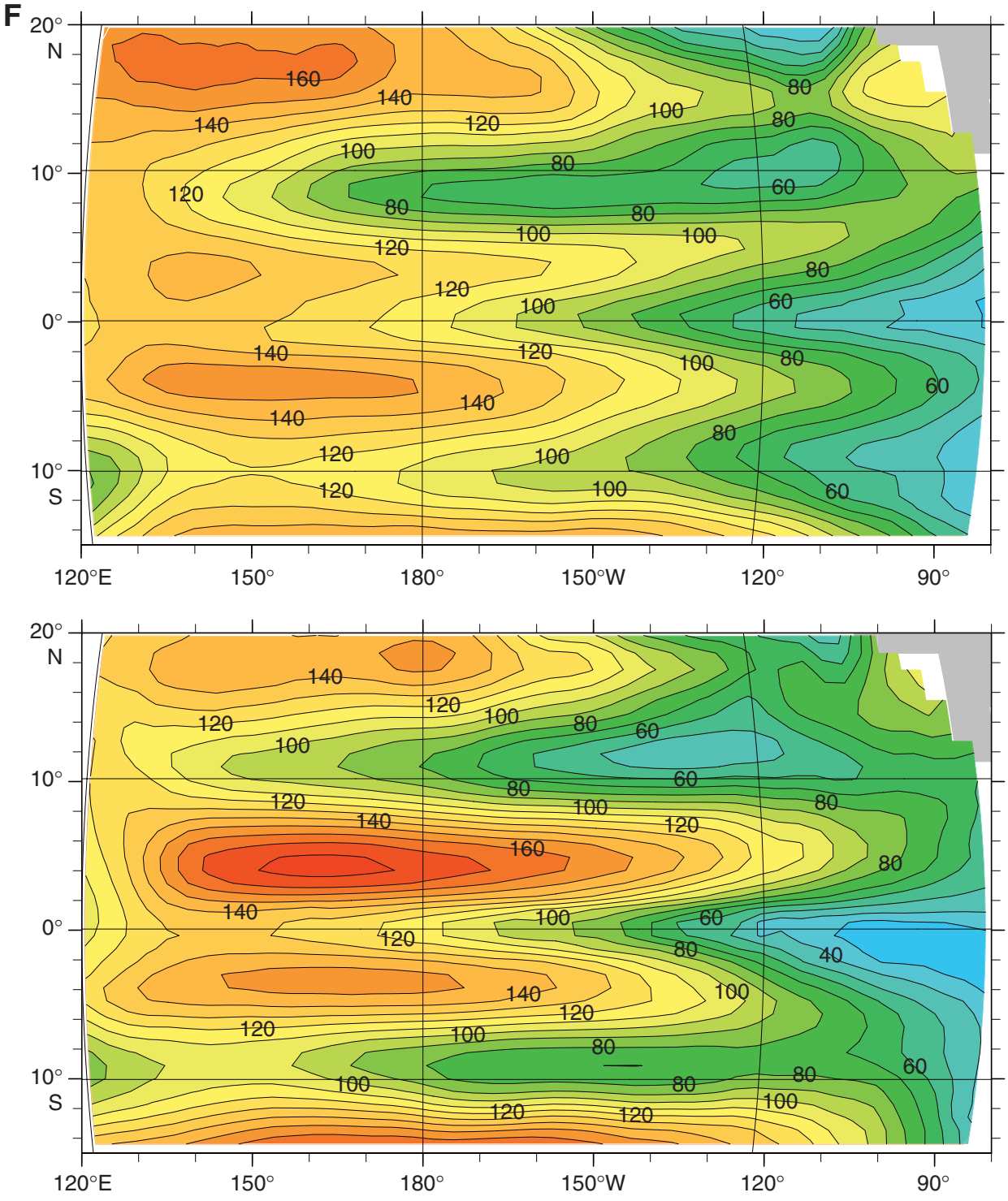

Figure F3 (continued). G. Transects of temperature along the equator at 5°S and 10°N for two seasons. AMJ = April, May, June; OND = October, November, December.

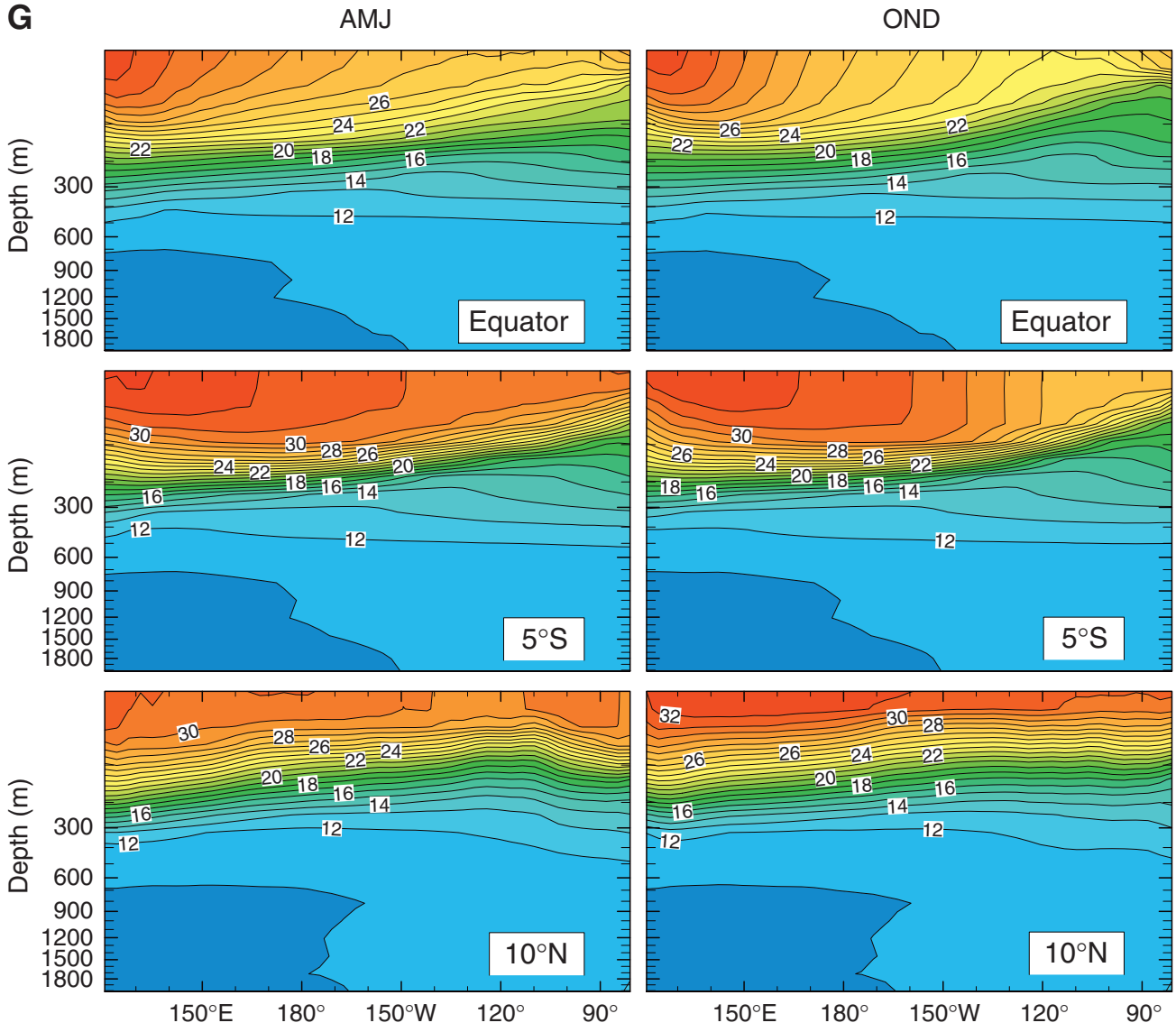

Figure F3 (continued). H. Estimated δ_c averaged annually, averaged in the upper 30 m (top), and averaged between 60 to 160 m (bottom).

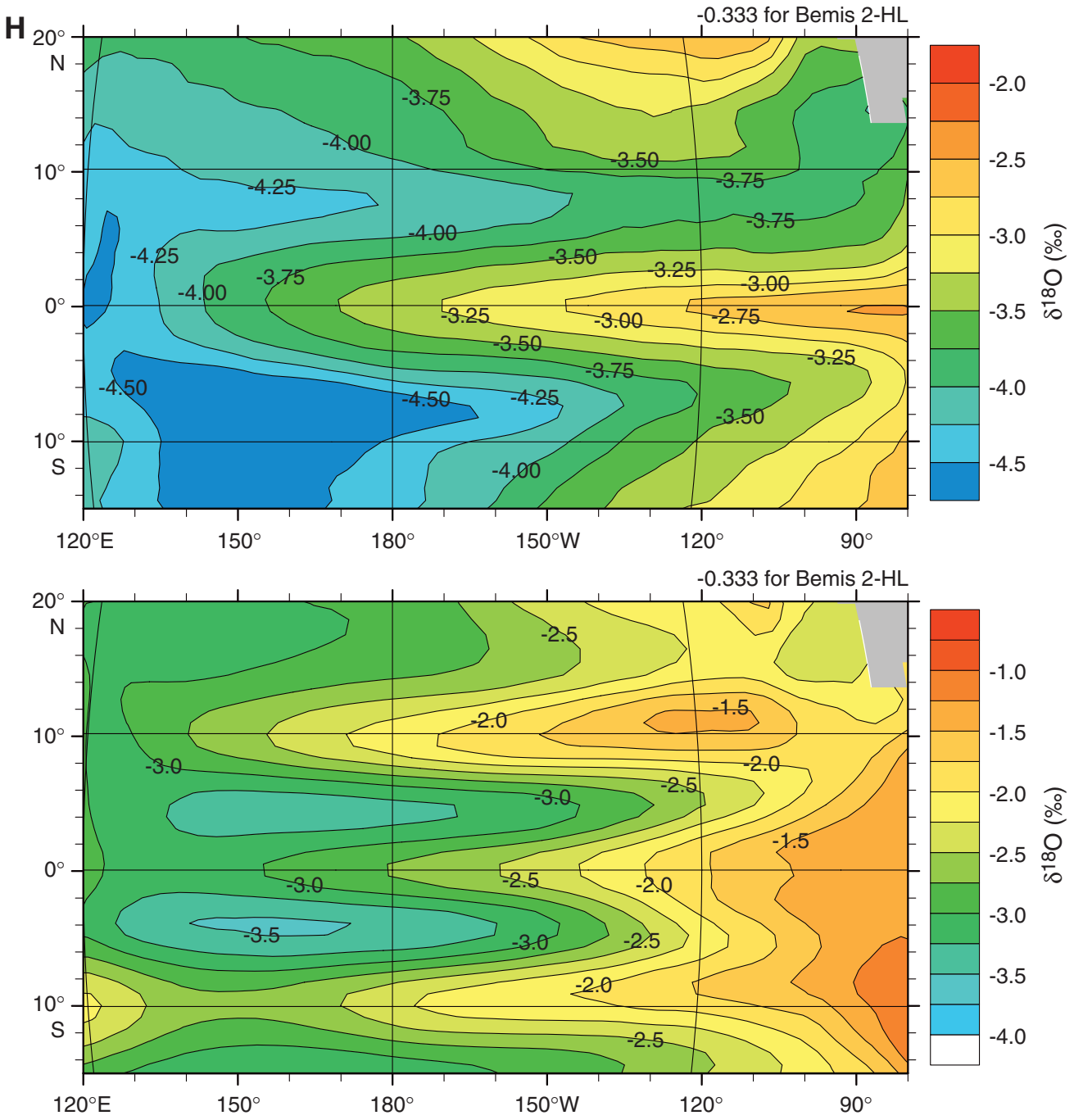

Figure F4. A. The annual average temperature and streamlines (top) and salinity and current vectors (bottom) for the thermocline layer (60–160 m). (Continued on next two pages.)

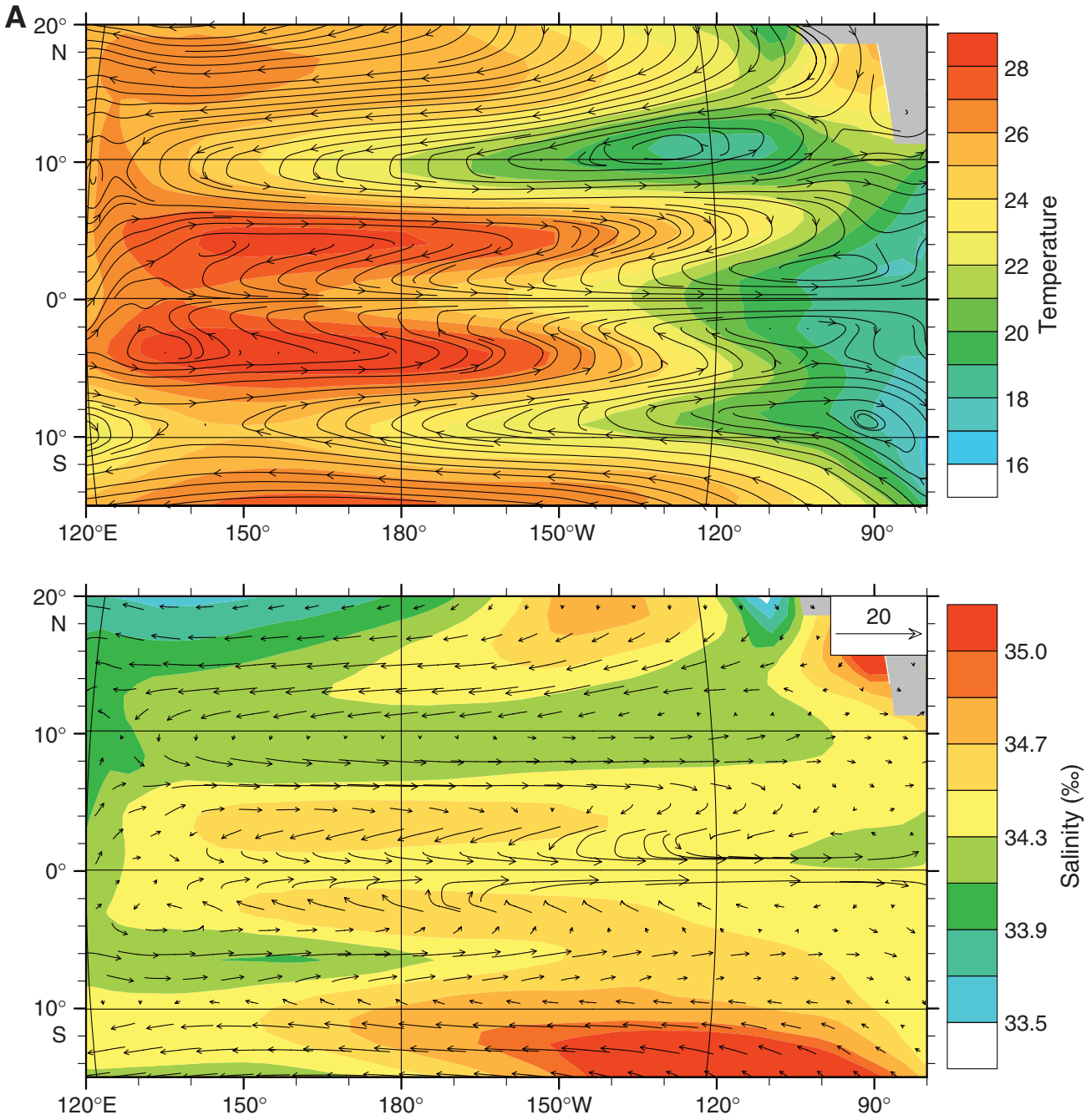

Figure F4 (continued). B. AMJ temperature and streamlines (top) and AMJ salinity and current vectors (bottom) at 60–160 m.

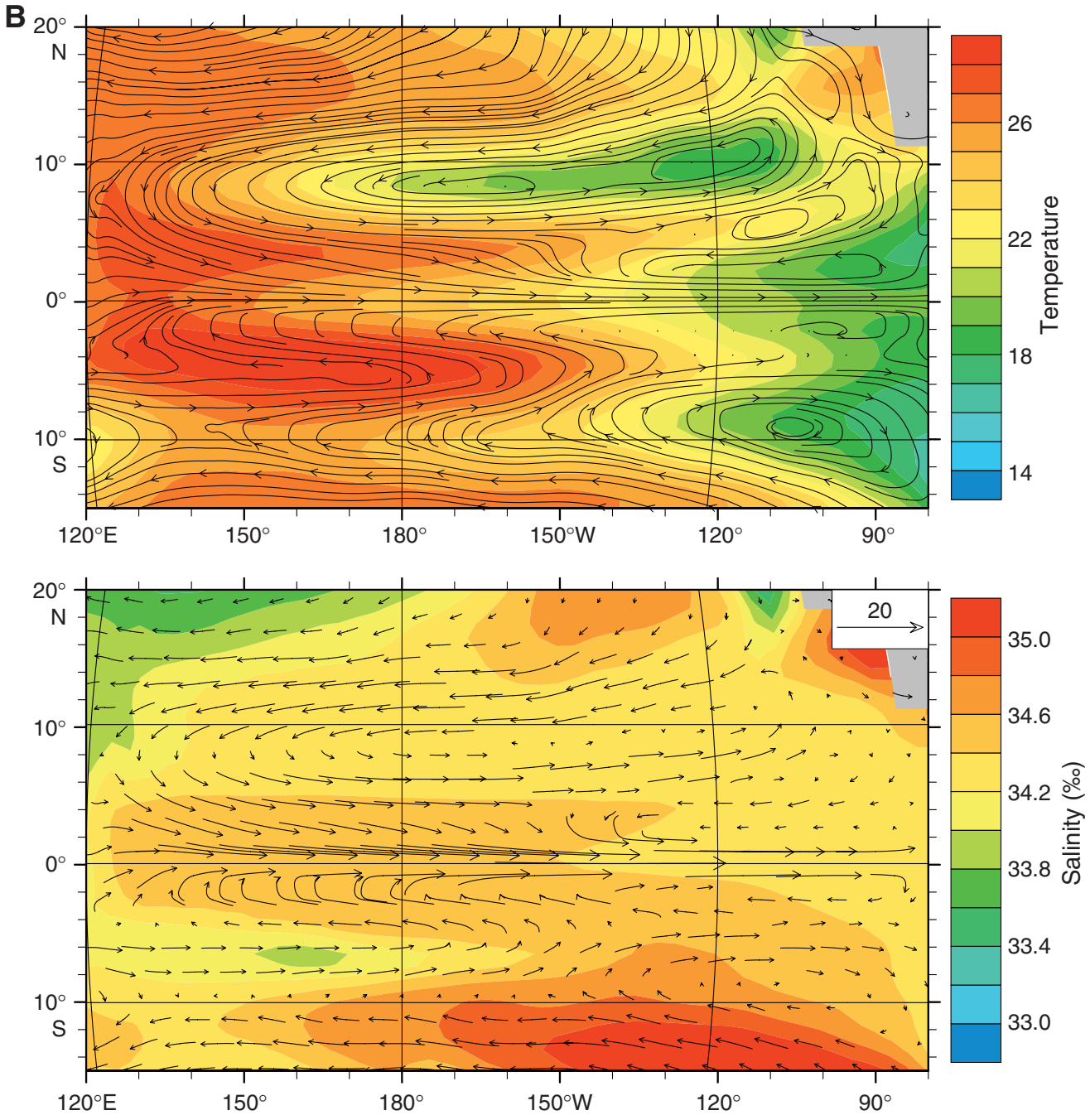

Figure F4 (continued). C. OND temperature and streamlines (top) and OND salinity and current vectors (bottom) at 60–160 m.

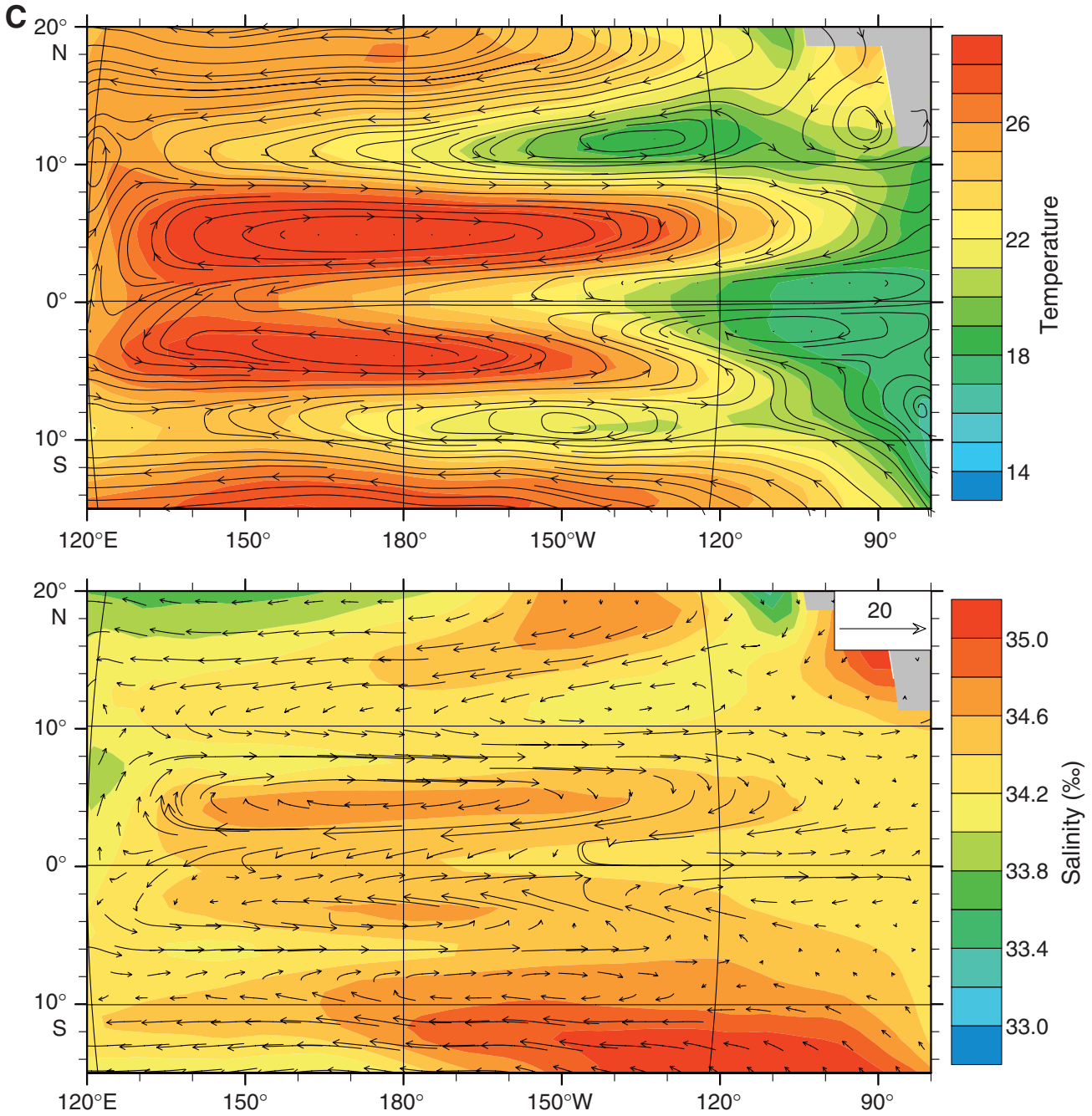

Figure F5. The annual average of temperature and streamlines (top) and salinity and current vectors (bottom) for 190–550 m.

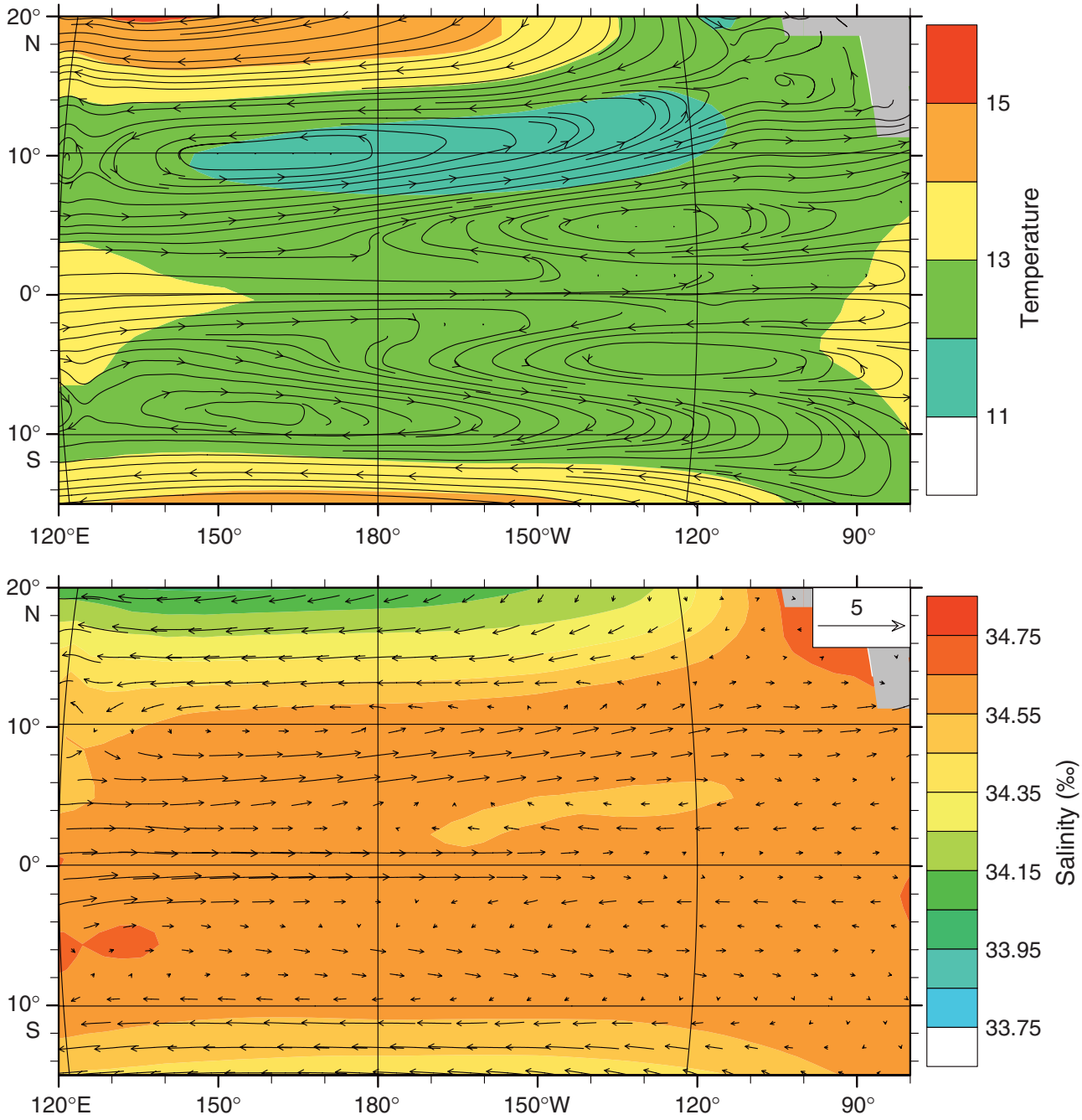

Figure F6. The annual average temperature and streamlines (top) and salinity and current vectors (bottom) for 900–2000 m.

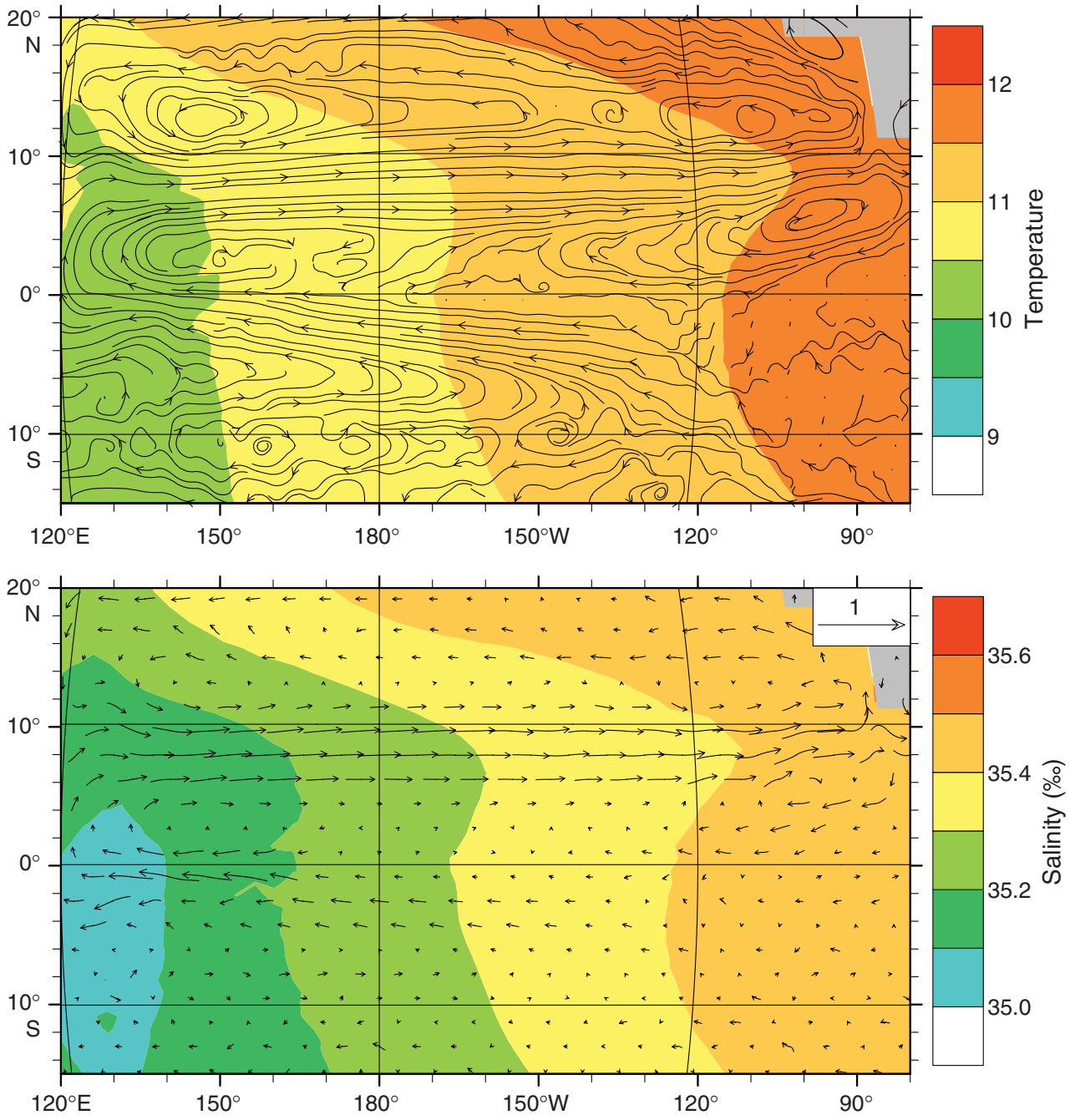

Figure F7. A. The AMJ meridional transects along 115°W showing the east-west velocity (in centimeters per second) (top) vs. seasonal average temperature and estimated δ_c‰ relative to Peedee Belemite (PDB) (bottom). (Continued on next page.)

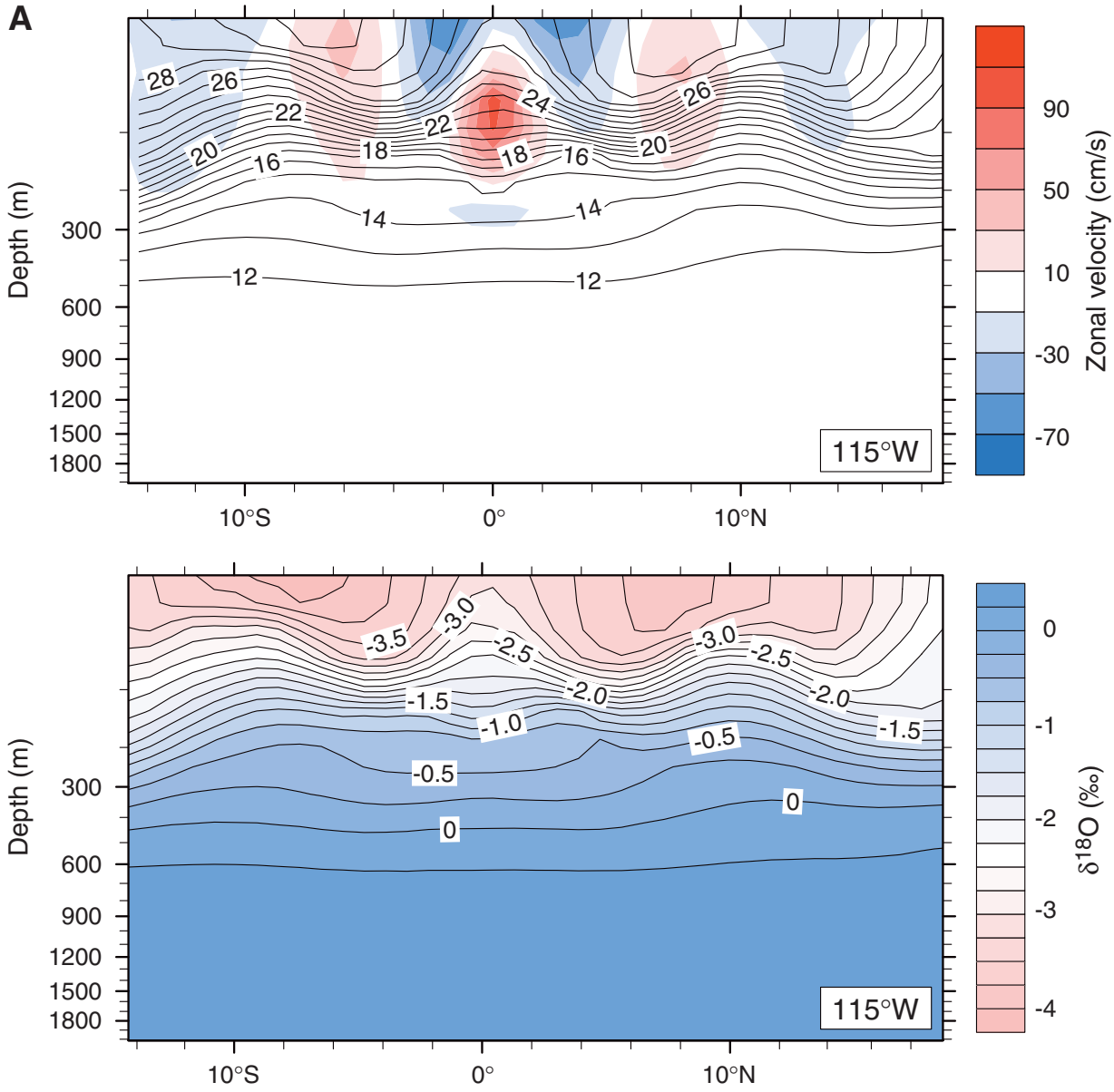

Figure F7 (continued). B. The OND meridional transects along 115°W showing the east-west velocity (centimeters per second) (top) vs. seasonal average temperature and estimated δ_c per milliliter relative to OND (bottom).